OPEN ACCESS

Phase transitions far from equilibrium in wet granular matter

New Journal of Physics
The open-access journal for physics

Phase transitions far from equilibrium in wet granular matter

A Fingerle, K Roeller, K Huang and S Herminghaus[1]
Max Planck Institute for Dynamics and Self-Organization, Bunsenstrasse 10, 37073 Göttingen, Germany
E-mail: axel.fingerle@ds.mpg.de, klaus.roeller@ds.mpg.de, kai.huang@ds.mpg.de and stephan.herminghaus@ds.mpg.de

New Journal of Physics **10** (2008) 053020 (10pp)
Received 28 January 2008
Published 15 May 2008
Online at http://www.njp.org/
doi:10.1088/1367-2630/10/5/053020

Abstract. The phase diagram of vertically agitated wet granular matter is presented, both experimentally and by simulation. We observe two phase transitions, one of which is driven by the applied force (acceleration), the other by injected energy (velocity of container walls). All observed features can be traced down to the hysteretic nature of capillary bridge formation and rupture. Other details of the interaction are remarkably irrelevant, suggesting a certain universality for the investigated phenomena.

Phase transitions in condensed matter under thermally equilibrated conditions are by far the best understood examples of collective behavior. The astonishing fact that a solid melts at a precisely defined temperature, although the thermal energy is broadly distributed among the many degrees of freedom, can be completely apprehended from the principle of free energy minimization. Furthermore, the role of thermal fluctuations, which lead to the striking universality near critical points, was cast into a closed theory by means of the renormalization group [1]. Hence, the physics of phase transitions at thermal equilibrium has matured into solid textbook knowledge (see, for instance [2]).

Phase transitions far from equilibrium, on the contrary, are still far from being understood on such a general basis, despite their ubiquity and striking similarity. Well-known examples that are currently of great interest range from collective pattern formation in systems of molecular [3] and micron scale [4, 5] to transitions in social behavior [6]–[8]. In particular, dynamic transitions in granular matter, such as soil liquefaction due to earthquakes, fluidization by vibration, or phase separation ([9]–[18]; [19] and references therein) are examples in systems of great practical interest. As the strength of the external drive is varied, sudden changes in the

[1] Author to whom any correspondence should be addressed.

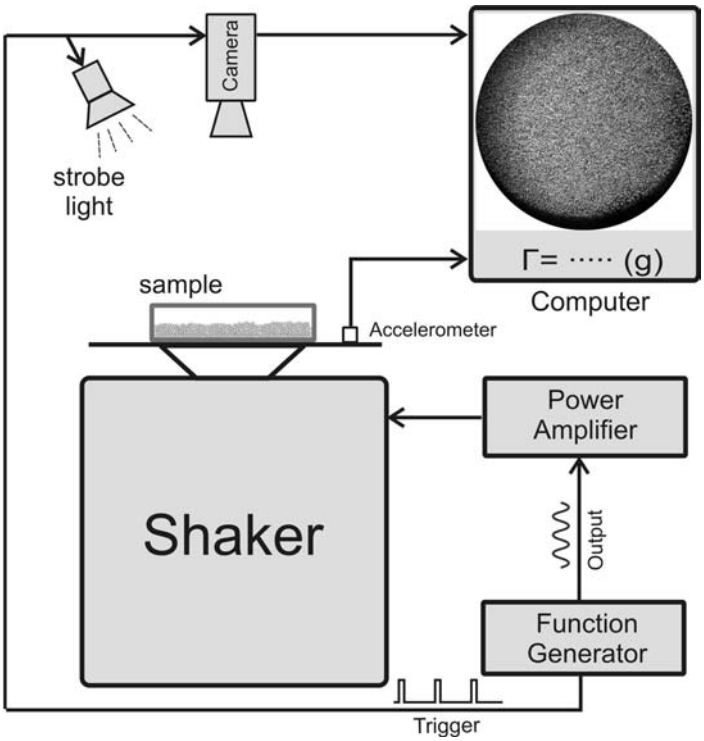

Figure 1. Sketch of the experimental set-up. Strobe light illumination enables accurate assessment of the phase boundary between the solid and the liquid phase. Image acquisition with a well-defined time lapse is necessary as well for a reliable determination of the (spatially varying) granular temperature.

dynamical behavior of the granulate can be observed. Furthermore, it has become apparent that *wet* granular matter provides a particularly well-suited model system for the study of such phenomena [19]–[21]. The main difference between dry and wet granular systems is that in the latter, liquid capillary bridges forming between adjacent grains provide a well-defined energy scale determined by the surface tension of the liquid [19, 22]. In the present paper, we analyze the dynamics of wet granular matter under vertical agitation in a closed container. We present the phase diagram and demonstrate that many of its features are quantitatively independent of the details of the 'microscopic' interaction mediated by the capillary bridges. This may be viewed as some kind of universality in its own right.

As a well-defined granular system, we chose spherical glass beads (density of the glass $\approx 2.5\,\mathrm{g\,cm^{-3}}$), which can be purchased in large quantities and with reasonable quality. They are widely used as model granulates and thus provide good comparability with other studies. The average diameters of the spheres ranged from 0.5 to 1.5 mm. The width of the size distribution was about 10% of the average diameter in each sample. As the liquid, we used water in most experiments, and sometimes *n*-nonane for comparison. Both liquids wet the glass surface well, with a contact angle below 10°. The main difference is the surface tension, γ, which is $72\,\mathrm{mN\,m^{-1}}$ for water and $24\,\mathrm{mN\,m^{-1}}$ for nonane. This allows for comparing strongly different rupture energies of the capillary bridges. A wide cylindrical container (14 cm diameter petri dish with lid, cf figure 1) was used in order to eliminate side wall effects, which had been reported to dominate fluidization in narrow containers [21]. The petri dish was filled to about two-thirds of its height with granulate, mounted on an electromagnetic vertical shaker, the lid closed and set in

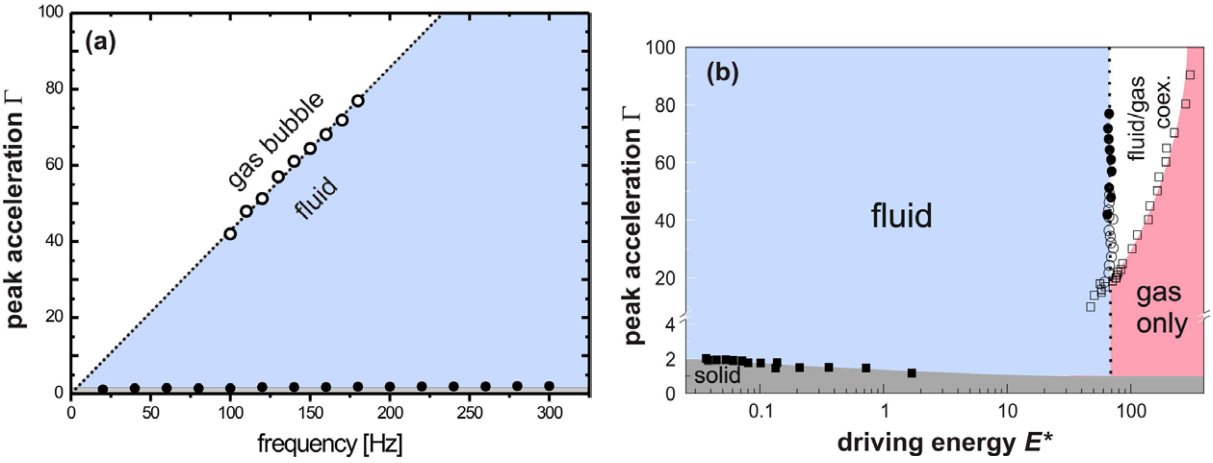

Figure 2. (a) Experimental phase diagram of wet granular matter under vertical agitation ($R = 850\,\mu$m, $w = 0.41\%$; water as the liquid). (b) Same as (a), but presented in the plane spanned by the parameters Γ and E^*. The data for water (closed) and *n*-nonane (open) collapse in this plot. Note that the vertical scale has been split for proper presentation of the solid/fluid phase boundary.

oscillatory motion, $z(t) = A\cos(2\pi\nu t)$. The dimensionless peak acceleration, $\Gamma = 4\pi^2 A\nu^2/g$ (where g is the acceleration due to gravity) serves as a control parameter. Typical frequencies are a few hundred Hertz. For Γ below and around one, the gravitational force on the granular pile, as viewed in the rest frame of the petri dish, is always pointing downwards, although sinusoidally varying in magnitude. As a consequence, the grains are never lifted from their support, and the position of each grain within the sample remains fixed [9]. This represents a solid condensed state. It should be noted that the capillary bridges are much smaller than the glass beads, and thus small as compared to the capillary length of the liquids used, which is around 2 mm.[2] Gravity effects on the distribution of the liquid can thus be safely neglected.

As Γ is increased above unity by increasing A, the pile periodically experiences a lifting force. For a dry granulate, this leads to fluidization at a certain threshold, $\Gamma_c \approx 1.2 =: \Gamma_{dry}$ [9]. It manifests itself by the onset of a mild movement of the grains, as revealed by direct visual inspection. As liquid is added to the granulate, Γ_c increases strongly. This corresponds to the dramatic difference in mechanical strength observed between a dry granulate, which flows almost like a liquid, and the visco-plastic texture of a wet granulate [19]. It was shown before that the increase in Γ_c can be well understood from the attractive interaction due to the liquid capillary bridges forming between adjacent spheres [19, 21]. In particular, the excess $\Gamma - \Gamma_{dry}$ must be just large enough to overcome the forces exerted by these bridges by virtue of the surface tension of the liquid. Confirming earlier measurements [21], we found Γ_c to be largely independent of frequency. This can be clearly seen in figure 2(a), where the closed circles indicate the transition between the solid (below, gray) and the fluidized (above, blue) state.

At sufficiently high Γ, we could observe an additional transition, which is indicated by the open circles in figure 2(a). Above this line, a dense fluidized phase coexists with a dilute gas-like phase. The latter shows up as a 'gas bubble', an example of which can be seen in

[2] The capillary length is given by $\sqrt{\gamma/\rho g}$, where ρ is the density of the liquid. It is 2.7 mm for water and 1.7 mm for *n*-nonane.

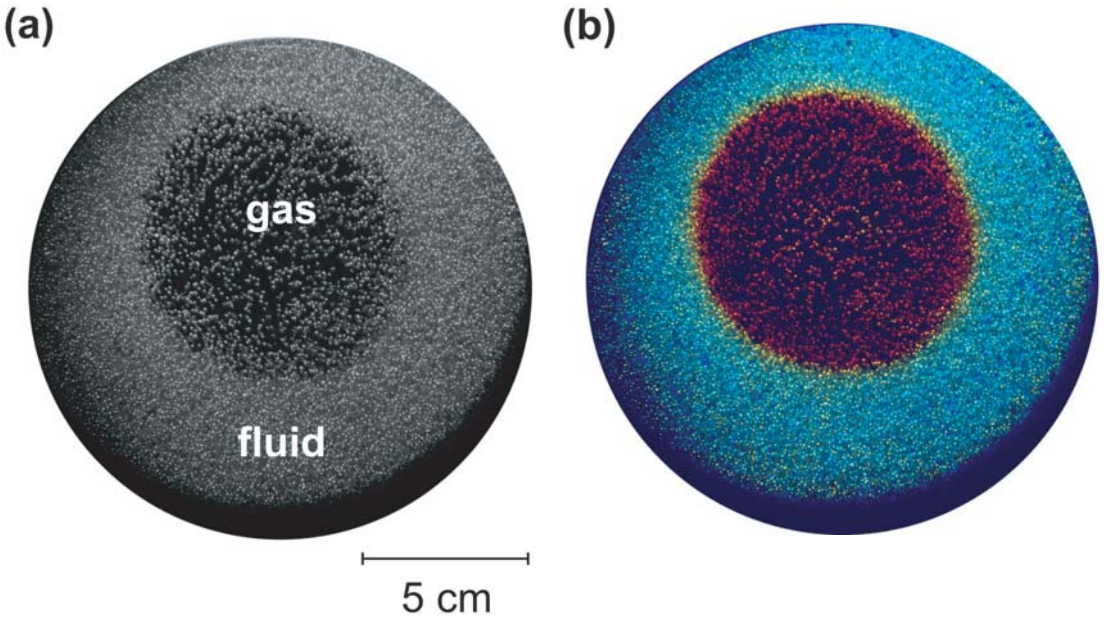

Figure 3. Fluid-gas coexistence. (a): top view of the experimental set-up at high excitation. The petri dish is illuminated from above and observed in reflection. The glass spheres appear as bright dots. In the middle of the sample, a large gas bubble is clearly visible, while the outer part is filled with a condensed fluidized phase (a video is available online[3]). (b): same snapshot as in (a) but colored according to temporal autocorrelation. The color scale extends from blue (slow movement) to red (fast movement).

figure 3. The bubble is found to sometimes wander around in the container, which shows that its presence is not linked to a lateral inhomogeneity in the excitation amplitude, but is intrinsic to the system under study.

In order to assess the granular temperature in either phase, i.e. the average kinetic energy of the glass beads, we determined their velocity qualitatively by means of a simple autocorrelation procedure. Images were taken with a fast video camera at two consecutive periods of the agitation. They were subtracted from each other, and the square of the result was taken, in order to obtain a measure for the temporal changes in brightness. This was averaged over areas small enough to contain not more than one bead at a time (5×5 pixels). The result, which qualitatively captures the horizontal component of the velocity, was encoded in color, with blue corresponding to little movement and red corresponding to strong movement. The color scale extends to about $3\,\mathrm{cm\,s^{-1}}$ at dark red. Clearly, a large difference in the granular temperature is found between the gas phase and the fluid phase. This is in sharp contrast to two-phase coexistence as commonly known from equilibrium systems, where temperature is uniform in the steady state.

An obvious feature of figure 2(a) is that the data suggest the phase boundary between the fluid-state and the fluid-gas coexistence to be a straight line meeting the origin of the diagram (dotted line). The quantity Γ/ν, which is proportional to the peak velocity of the container walls, is constant along this line. This is interesting in view of earlier experiments using a different

[3] See stacks.iop.org/NJP/10/053020/mmedia 'Experiment'. The frame rate in the movie is equal to the shaking frequency ($50\,\mathrm{s^{-1}}$). The particles are 1.09 mm diameter glass beads, wetted by water.

agitation scheme [14], where a pronounced transition, reminiscent of condensation from a gas into a viscous fluid, occurred when the peak velocity of the container walls came below a critical value, v_c. This value was found to correspond to the kinetic energy a bead must have in order to rupture the liquid bridge binding it to a neighboring bead. It is given by $\frac{m}{2}v_c^2 = E_{cb}$, where m is the mass of the glass bead and $E_{cb} \propto R^2\gamma\sqrt{w}$ is the energy needed to rupture a capillary bridge [19], [23]–[26]. R is the radius of the beads and w denotes the liquid content of the sample, defined as the volume of the added liquid divided by the total volume of all glass spheres. Following this view, it is convenient to introduce the characteristic dimensionless 'driving energy', $E^* := \frac{m}{2}v^2/E_{cb}$, where $v = 2\pi A\nu$ is the peak velocity of the container walls (bottom and lid in our experiment). E^* corresponds to the typical energy of a bead close to the container wall in a dense granulate, where the motion of the walls largely determines the velocity of the glass beads close to it. E^* will henceforth be considered as an alternative control parameter. By varying A and ν, the two parameters Γ and E^* can be controlled independently.

It is enlightening to plot the loci of the observed transitions in the plane spanned by Γ and E^*. The result is shown in figure 2(b). The transition from the solid (gray) to the fluid phase (blue) is represented by a more or less horizontal line, indicating that this transition is independent of energy, but driven by acceleration (Γ). In contrast, the fluid phase is separated from the fluid/gas coexistence region (white) by a vertical line, indicating a transition driven by injected energy (E^*), but independent of force. The perfect matching of the data obtained for water (closed) and n-nonane (open), the surface tension of which is a factor of 3 smaller than that of water, strongly suggests that our scaling of the driving energy with respect to the bridge rupture energy, E_{cb}, is physically appropriate. As the amplitude was further increased, the container was finally filled homogeneously with a hot gas phase. This is represented as the red shaded area in the figure.

In order to demonstrate the essential role of the capillary bridges, we performed molecular dynamics type simulations in two-dimensions (2D) with ideally circular, frictionless discs mimicking the glass beads. The attractive pairwise *hysteretic* interaction potential [19, 21] illustrated in the inset of figure 4 models the capillary bridges (dotted: approach and solid: retract). The repulsion between particles is modeled by a Hertz-potential ($\propto (-s)^{5/2}$), which is turned on for negative s only. The bridge is thus assumed to exert a constant force upon retraction, and to rupture at a distance s_c. A gravitational force acting in the vertical direction is included in the simulations as well. The liquid content per grain is assumed to be the same everywhere. This is justified from the experimental observation that the liquid distributes rapidly in the sample, and quite evenly on each sphere after impact [27]. At the top of figure 4, a snapshot of a 2D stationary state is shown, as obtained by 2D simulation (one lateral and one vertical coordinate). It is clearly seen that the simulation produces a dense plug as well as a gaseous region, which are in coexistence with each other.

In the main panel of figure 4, the density as well as the granular temperature, $T = \langle E_{kin}\rangle$, in units of the rupture energy, E_{cb}, are plotted as a function of the lateral coordinate, on the same scale as the simulation box above. The granular temperature is found to vary over two orders of magnitude. This clearly demonstrates, in accordance with the experiment, that the observed phenomenon is by no means akin to coexistence between thermodynamic phases, but is an intrinsically non-equilibrium state. The appearance of a cold dense phase in coexistence with a dilute hot phase complies qualitatively with earlier results obtained with *magnetically* cohesive granular beads [15]. Although that system does not exhibit a defined energy loss scale, as opposed to the system we study here, the essential feature is similar: in the dense phase,

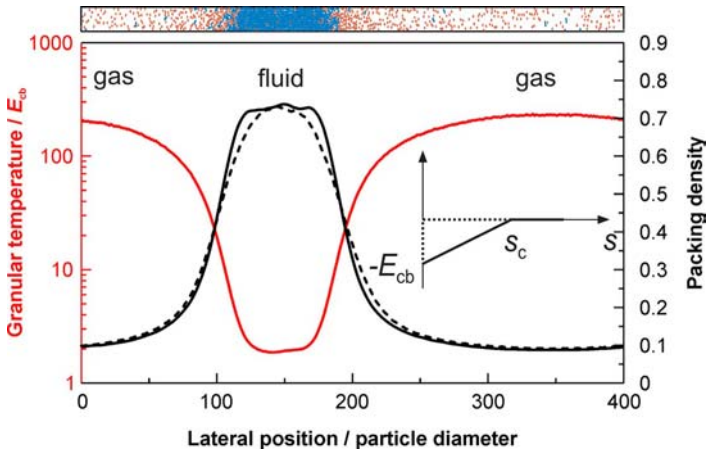

Figure 4. Box on top: snapshot of molecular dynamics type simulation of 1200 particles at parameters where fluid/gas coexistence occurs (a video is available online[4]). Blue grains have at least one liquid bridge, red grains have none. Main panel: plot of the granular temperature (red curve) and the number density (solid black curve) on the same scale as the simulation box above. The temperature varies laterally over two orders of magnitude, being high in the gas, but very low within the fluid plug. The density is also shown for event-driven simulations (dashed black curve, square well potential).

where the mean free path is small, the collision frequency is high. This gives rise to strong dissipation, and hence to very effective cooling.

Figure 5(a) shows the phase diagram as obtained from the simulations, in the same plane as figure 2(b), but on log/linear scale to better reveal the details. We clearly see the horizontal line separating the solid (gray) from the fluid phase (blue) or, at higher E^*, form a solid/gas coexistence (white). As found in the experiments, the fluid phase is separated from the fluid/gas coexistence by a vertical line. The fluid/gas coexistence region is bounded by a second line located at larger driving energy, which indicates the transition to a homogeneous gas-like state (red). In this transition line, a bulge is observed where the excitation amplitude A equals the rupture length s_c of the capillary bridges. Unfortunately, scaling the simulation parameters according to the experimental conditions (note that the simulation is 2D) reveals that this bulge is just out of the range accessible to our experimental set-up.

In figure 5(b), we replotted the coexistence region in the plane spanned by the driving energy, $\frac{m}{2}v^2$, and the capillary bridge energy, E_{cb}. We rescaled them as $\tilde{E}_{kin} := mv^2/2F_g s_c = v^2/2gs_c$ and $\tilde{E}_{cb} := E_{cb}/F_g s_c$, respectively. Obviously, $\tilde{E}_{kin} \propto E_{cb}$ for both transition lines, supporting that this transition is exclusively governed by the bridge rupture energy. The gravitational energy scale naturally separates out, in contrast to dry granulates [16]. The only marked difference between the simulation (figure 5(a)) and the experiment (figure 2(b)) is the value of E^* at which the fluid phase region ends.

This discrepancy can be removed by considering the impact of the inelasticity of the glass beads used in the experiments. Their restitution coefficient, ε, as determined experimentally for particle–wall collisions, was found to be $\varepsilon \approx 0.90 \pm 0.01$. Including this inelasticity in our simulations, we observed that the critical line shifted towards higher driving velocities by a

[4] See stacks.iop.org/NJP/10/053020/mmedia 'Simulation 2D'.

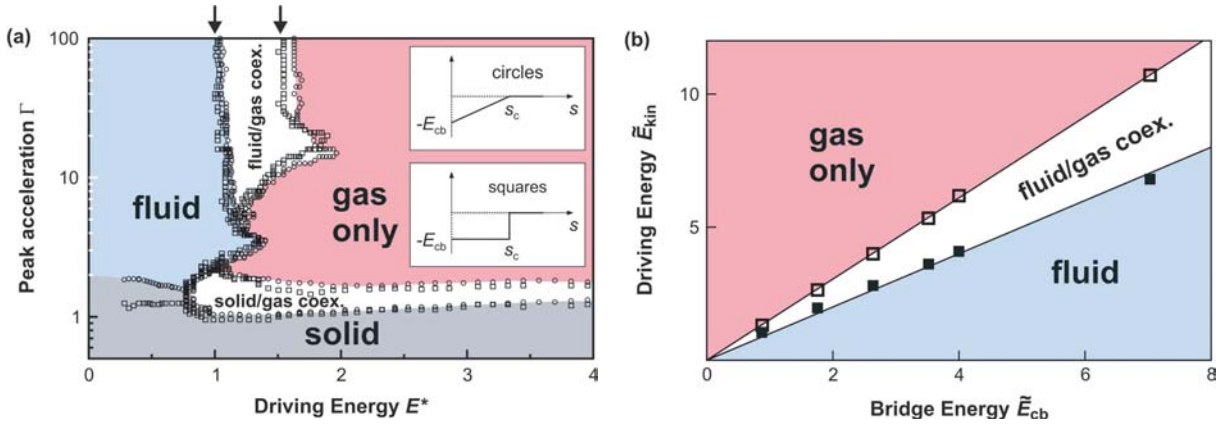

Figure 5. (a) Phase diagram from simulations with 1200 particles in 2D. The horizontal boundary of the solid phase is clearly obtained, as well as the vertical fluid/gas boundaries which are also seen in the experiment. The arrows at the top indicate the slopes of the lines in the inset of (a). The insets show the hysteretic interaction potentials chosen (dotted: approach and solid: retract). (b) Variation of the transition points with the surface tension, as obtained from our simulations. The transition energies scale precisely with E_{cb}. The slopes yield the critical (scaled) driving energies E^* as 1.00 ± 0.09 and 1.52 ± 0.02, respectively (arrows in (a)).

factor of 7.3 in 2D, and by a factor of 31 in 3D. Qualitatively, the phase diagram remained unchanged. Note that the characteristic Y shape of the phase boundaries, which is qualitatively observed in the experiment as well (figure 2(b)), entails the existence of a tricritical point at the lower tip of the coexistence region. It is of great interest how this compares to similar phenomena known from equilibrium physics [28, 29]. This will be the focus of a forthcoming study.

In order to investigate whether the observed behavior is of appreciable universality, we varied the interaction potential used in the simulations. In figure 5(a), the circles represent simulations assuming a constant capillary force upon retraction (triangular potential well, upper inset), while the squares were obtained assuming a square-well retraction potential, representing the limiting case of a delta-function force located at the rupture distance (square well, lower inset). As the figure clearly shows, even these extreme cases give almost identical results. The only significant difference is the position of the solid/fluid transition at small driving velocities, which is expected due to the vanishing contact force for the square-well potential. The other details found in the phase transition lines do not seem to depend crucially on the interaction characteristics. The only relevant ingredient of the latter is their being dissipative in the proposed hysteretic sense.

A particular significance of the square-well potential is that it leads to vanishing forces, except for a set of zero measure on the time axis. This enables event-driven simulations, which are much more economic in computational power than the full integration of the equation of motion. For the square-well potential, we can thus perform simulations with very many particles, and in 3D. For these simulations, we used hard-core repulsion between the particles. A 3D simulation at parameters corresponding to fluid/gas coexistence is shown in figure 6(a). The similarity with the experimental results displayed in figure 3 is obvious. As

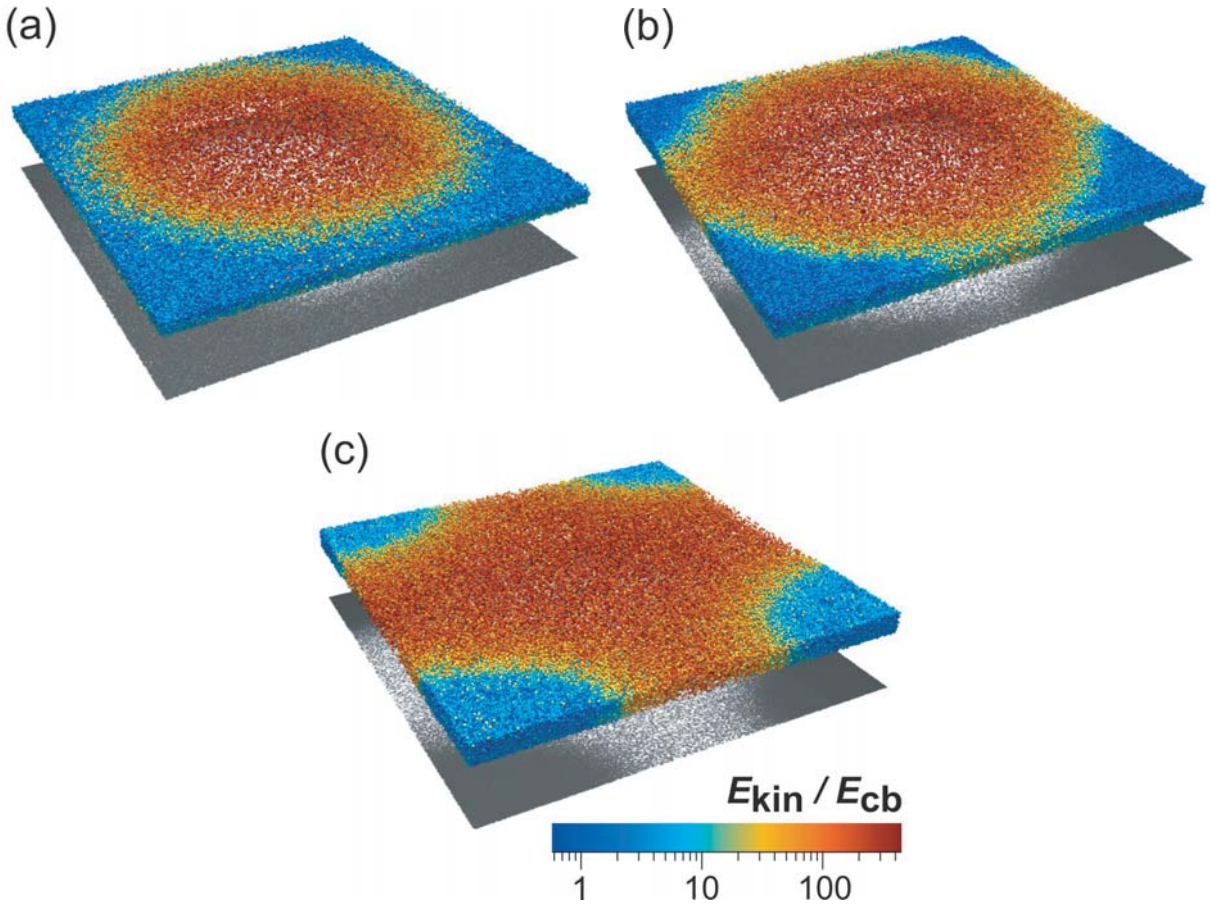

Figure 6. Snapshots of event-driven 3D simulations at early (a), intermediate (b), and late (c) stage (a video is available online[5]). The color indicates the kinetic energy of the grains, similar to figure 3(b). The 'shadow' is computed such as to imitate illumination from above, in order to account for the areal density of the particles (dark regions correspond to high density).

we let the bubble expand to system size, it finally reaches the boundaries of the box. Due to the periodic boundary conditions, this corresponds to a diamond-shaped condensed region centered at the corner between four adjacent replicas of the simulation boxes (figure 6(b)). Figure 6(c) shows the situation somewhat later. Clearly, the diamond shaped condensate region has rounded to a circular spot, strongly suggesting the presence of an interfacial tension. It appears prospectively interesting to investigate this in detail, since interfacial tensions are usually defined as equilibrium free energies, which certainly does not apply here. We note in this context that the force law has some noticeable influence on the interfacial density profile, as shown in figure 4 by the solid (triangular well, full integration) and dashed (square well, event driven) black curve.

Let us try to understand our findings in a more general framework. From the 'traditional' conditions invoked for the description of equilibrium phase transitions, only the homogeneity of the lateral pressure carries over to driven steady states, due to the required force balance at the phase boundaries. In contrast, the familiar uniformity of temperature breaks down. In what

[5] See stacks.iop.org/NJP/10/053020/mmedia 'Simulation 3D'.

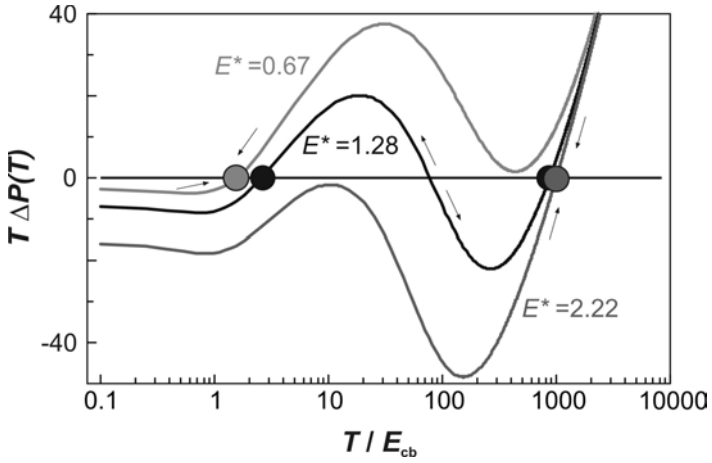

Figure 7. The net power, $\Delta P = P_{\text{diss}} - P_{\text{inj}}$, as a function of the granular temperature. ΔP is multiplied by the granular temperature here in order to achieve a clear presentation of data in a single graph. Depending on the driving energy E^*, we obtain either one (gray) or two (black) stable zeros, corresponding to a single phase or two-phase coexistence, respectively. The arrows denote the response of the system to small fluctuations.

follows, we ask for the mechanism by which the symmetry in the formerly homogenous system is broken, and how the system finds its steady state within the broken symmetry.

The power injected into the system from the oscillating walls, P_{inj}, must be balanced at each lateral position within the sample by dissipation, P_{diss}. Assuming a certain[4] velocity distribution for the grains, both quantities can be evaluated in a straightforward way, such that the net power $\Delta P(T) = P_{\text{diss}} - P_{\text{inj}}$ can be obtained as a function of temperature [20]. Clearly, in a dissipative system like the one under study, the velocity distribution will in general deviate from the 'usual' Gaussian [30, 31], exhibiting non-Gaussian 'tails'. However, these affect only a small fraction of the particles [31, 32] and are of minor impact on the average collision frequency, which in turn determines the dissipation rate. In order to compute the abovementioned quantities, it thus appears sufficient to use a Gaussian velocity distribution for the sake of simplicity.

Figure 7 shows the obtained result, displayed for three values of the driving energy, E^*. For $E^* < 0.67$, we obtain just one stable (i.e. positive slope) zero, which is at low temperature. It corresponds to a moderately dense state, which has just enough free volume for the critical separation s_c to be exceeded frequently enough to balance the injected power, P_{inj}. On the other hand, for $E^* > 2.22$, we have again only one stable zero, but this corresponds to a high temperature. It represents a dilute phase, the temperature of which is determined mainly by the balance of the energy uptake from the motion of the boundaries with the dissipation due to the 'wet' impacts with them.

At intermediate velocities (black curve in figure 7), two stable zeros (black circles) are obtained, one for low and one for high temperature. This is to be identified with the fluid/gas coexistence observed in the simulations as well as in the experiments for intermediate velocities. Since this continuum theory does not take gravity into account, it is intrinsically independent of the parameter Γ used in figure 5, and thus corresponds to the vertical lines in the phase diagram. The mean field model predicts the coexistence in the stripe $0.67 < E^* < 2.22$ of the

phase diagram, which compares quite favorably with figure 5(b) for $\Gamma \gg 1$ (where gravity is irrelevant) given the crudeness of the involved assumptions.

We thus have shown by experiments, simulation and analytical theory that the phase diagram of wet granular matter under vertical agitation can be quite well understood on the basis of a very simple model, which only takes the hysteretic formation and rupture of capillary bridges into account. The weak dependence of the phase diagram on details of this interaction is remarkable, and indicates significant universality of the obtained results.

Acknowledgment

Inspiring discussions with Stephan Ulrich, Annette Zippelius and Mario Liu are gratefully acknowledged.

References

[1] Wilson K G and Kogut J 1974 *Phys. Rep.* **12** 75
[2] Yeomans J M 1992 *Statistical Mechanics of Phase Transitions* (Oxford: Oxford University Press)
[3] Ertl G and Imbihl R 1995 *Chem. Rev.* **95** 697
[4] Fox J J, Gilmour R F Jr and Bodenschatz E 2002 *Phys. Rev. Lett.* **89** 198101
[5] Chakrabarti J, Dzubiella J and Löwen H 2004 *Phys. Rev.* E **70** 012401
[6] Farkas I, Helbing D and Vicsek T 2002 *Nature* **419** 131
[7] Vollmer J, Vegh A G, Lange Ch and Eckhardt B 2006 *Phys. Rev.* E **73** 061924
[8] Sumpter D J T 2006 *Phil. Trans. R. Soc.* B **361** 5
[9] Duran J 2000 *Sands, Powders, and Grains* (New York: Springer)
[10] Nagel S R 1992 *Rev. Mod. Phys.* **64** 321
[11] van der Weele K, van der Meer D, Versluis M and Lohse D 2001 *Europhys. Lett.* **53** 328
[12] Iveson S M, Litster J D, Hapgood K and Ennis B J 2001 *Powder Technol.* **117** 3
[13] Samadani A and Kudrolli A 2000 *Phys. Rev. Lett.* **85** 5102
[14] Geromichalos D, Kohonen M, Mugele F and Herminghaus S 2003 *Phys. Rev. Lett.* **90** 168702
[15] Blair D L and Kudrolli A 2003 *Phys. Rev.* E **67** 021302
[16] Götzendorfer A, Kreft J, Kruelle C A and Rehberg I 2005 *Phys. Rev. Lett.* **95** 135704
[17] Fingerle A and Herminghaus S 2006 *Phys. Rev. Lett.* **97** 078001
[18] Götzendorfer A, Kruelle Ch A, Rehberg I and Svensek D 2006 *Phys. Rev. Lett.* **97** 198001
[19] Herminghaus S 2005 *Adv. Phys.* **54** 221
[20] Fingerle A and Herminghaus S 2008 *Phys. Rev.* E **77** 011306
[21] Scheel M, Geromichalos D and Herminghaus S 2004 *J. Phys.: Condens. Matter* **16** S4213
[22] Mitarai N and Nori F 2006 *Adv. Phys.* **55** 1
[23] Willett Ch D, Adams M J, Johnson S A and Seville J P K 2000 *Langmuir* **16** 9396
[24] Lian G, Thornton C and Adams M J 1998 *Chem. Eng. Sci.* **53** 3381
[25] Mikami T, Kamiya H and Horio M 1998 *Chem. Eng. Sci.* **53** 1927
[26] Simons S J R and Fairbrother R J 2000 *Powder Technol.* **110** 44
[27] Fingerle A and Herminghaus S 2007 Mechanisms of dissipation in wet granular matter *Preprint* arXiv:0708.2597
[28] Leiderer P and Bosch W 1980 *Phys. Rev. Lett.* **45** 727
[29] Petrova A E, Krasnorusskii V N, Sarrao J and Stishov S M 2006 *J. Exp. Theor. Phys.* **102** 636
[30] Losert W *et al* 1999 *Chaos* **9** 682
[31] Rouyer F and Menon N 2000 *Phys. Rev. Lett.* **85** 3676
[32] Fingerle A, Scheel M and Herminghaus S Determining granular velocity distributions by Mössbauer spectroscopy, in preparation